A calibration bench to validate systematic error compensation strategies in hole drilling measurements

Marco Beghini[1], Tommaso Grossi[1*], Ciro Santus[1] and Emilio Valentini[2]

[1]*Department of Civil and Industrial Engineering, University of Pisa, Pisa, Italy*
[2]*SINT Technology Srl, Florence, Italy*

ABSTRACT

An accurate estimation of the measurement error in the hole drilling method is needed to choose an appropriate level of regularization and to perform a sensitivity analysis on the stress results. Latest release of ASTM E837 standard for the hole drilling method includes a procedure aimed at estimating the standard deviation of the random error component on strain measurements, proposed by Schajer. Nevertheless, strain measurements are also affected to some extent by systematic errors which are not included in the estimation and need to be compensated. For example, an error in the rosette gage factor or in the identification of the zero-depth point systematically affects all strain measurements in a strongly correlated fashion.
This paper describes a calibration bench, designed to superimpose a reference bending stress distribution on a given specimen while simultaneously performing a hole drilling measurement. Since the reference solution is known *a priori* and shares the measurement instrumentation, the hole geometry and the stepping process with the actual residual stress distribution, the bench provides the user with a direct validation of the obtained accuracy. In addition, strategies aimed at compensating systematic errors can be tested on the reference solution and then applied on the residual stress evaluation.
Two bias correction strategies are discussed and validated on a 7075-T651 aluminum specimen. It is observed that the imperfect hole geometry and drilling alignment lead to a significant underestimation of stresses near the surface. With the proposed bench, it is shown that this effect can be corrected.

Keywords: Residual stress, Hole drilling, Bench, Systematic errors

1. Introduction

The hole drilling method (HDM) [1]–[5] is a widely used technique for evaluating residual stresses, due to its relatively low cost and its in-field applicability. Commercially available devices such as MTS3000-Restan by *SINT Technology* provide the industrial user with suitable systems to perform the HDM ASTM procedure, E837 [5]. Its physical principle consists in the fact that drilling a hole in a stressed specimen produces strain relaxations in the material surrounding the hole. By measuring strains at increasing hole depths, the residual stress distributions along the depth, in the zone where the hole was drilled, can be obtained. Technical and mathematical details of the procedure can be found in Chapter 2 of Schajer's book [6].
Under the assumption of homogeneous isotropic linear elastic material, small strains, and plane stress state (due to the relatively low hole depth), the residual stress solutions can be obtained from a linear system of the form:

$$\boldsymbol{A}\boldsymbol{s} = \boldsymbol{e} \tag{1}$$

where $\boldsymbol{e}$ is a vector collecting the measured strains ε_i at various hole depths, $\boldsymbol{s}$ is a vector containing the identified residual stresses, and $\boldsymbol{A}$ is a calibration matrix – obtained through FEM analyses – which linearly connects the two vectors. A three strain gauges rosette is needed to identify a general plane stress state, and Schajer [3] showed that the three readings can be linearly combined to obtain three decoupled equations like Eq. (1). With the *Integral Method* (IM, [3], [4]), stress distributions are

* Corresponding author: tommaso.grossi@phd.unipi.it;

assumed to be piecewise constant functions, whose discrete values are stored in $\boldsymbol{s}$. Other general mathematical forms can be assumed to obtain a linear system like Eq. (1); for example, see the *Influence Functions Method* (IFM, [7], [8]) or the *Power Series Method* [3].
The HDM presents two mathematical peculiarities: 1) it gets severely ill-conditioned when the hole steps are reduced in size to obtain residual stresses with a finer spatial resolution; 2) relaxed strains at a given hole depth depend only on stress values at lower depths. The former implies that strain errors need to be characterized and properly mitigated. The latter means that when Eq. (1) is constructed through the IM, matrix $\boldsymbol{A}$ is lower-triangular, thus the identified stress values near the surface are determined by the first few values of measured strains.
Latest release of ASTM E837 standard includes a procedure to estimate random errors (namely, errors which affect every strain measurement randomly, such as electrical noise) and to filter them through Tikhonov regularization [9]. As observed in [10] and [11], strains are also affected by systematic errors which are not included in the estimation since they affect all measurements in a strongly correlated fashion, such as errors in the rosette gage factors or in the identification of the zero-depth point.
In Fig. 1 a calibration bench is presented, aimed at detecting and correcting these kinds of measurement biases by checking that the identified residual stresses match a known stress distribution. It has been designed and manufactured during a research collaboration between *SINT Technology* and the *Department of Civil and Industrial Engineering* at University of Pisa, as a development of the one described in [12].

2. Calibration bench

The bench is made up by a system which can impose a ≈ 40 mm vertical deflection by means of a pneumatic cylinder to the unsupported end of a 7075-T651 cantilever beam. The generated load is measured through a donut load cell, placed between the piston rod and the contact point with the specimen. The HDM procedure is carried out on the latter; its technical drawing is reported in Fig. 2. It has a tapered central section, and the load application point is determined so as to produce constant bending stresses on the upper and lower faces of the tapered region. The specimen material could be changed, as long as its thickness is adjusted in order to generate the desired values of bending stresses and piston load.

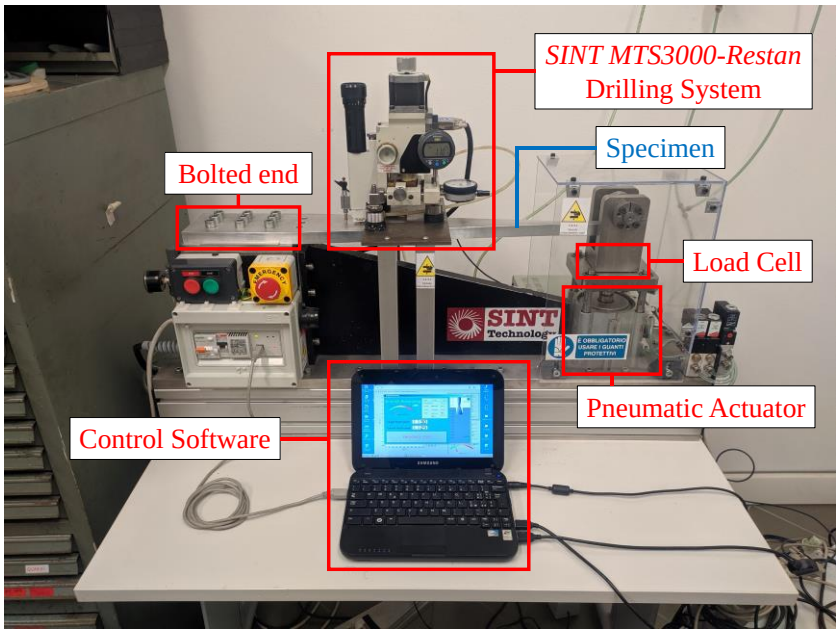

Fig. 1. Description of the calibration bench.

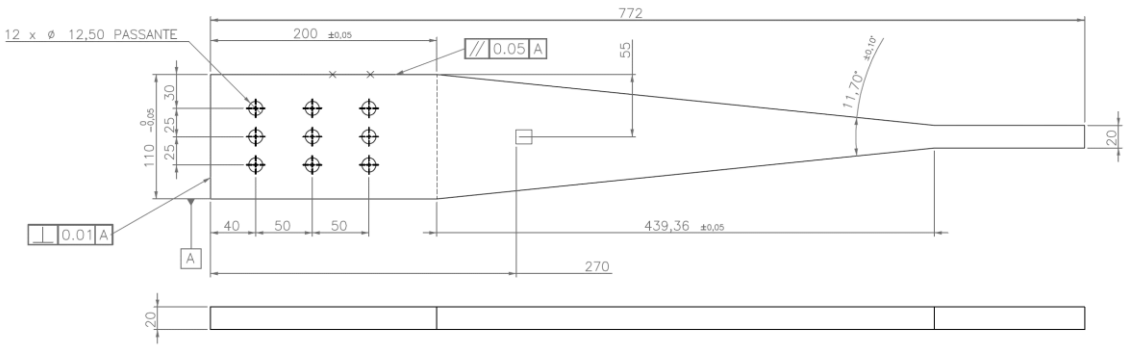

Fig. 2. Technical drawing of the specimen, realized in 7075-T651 aluminum. A conventional strain rosette position is reported, but it can be placed reasonably anywhere in the tapered region.

The HDM procedure is carried out with the MTS3000-Restan hole drilling equipment, produced by *SINT Technology*. Details of the system and of the test procedure are available in [13].
Through the pneumatic actuator, the external load can be applied and removed without disassembling any part of the system. This allows the user to measure *both* relaxed strains corresponding to bending stresses *and* relaxed strains corresponding to *actual* residual stresses in the specimen. Both stress distributions share their experimental setup, so they also share most of the factors which may introduce biases in the identification process. If biases are absent and random errors are properly filtered, the identified bending stress shall correspond to the applied distribution. Alternatively, the bench may be used to validate strategies aimed at correcting those biases.
In this work, two examples are provided. The first shows how the bench can be used to check the strain gauge setup and the material elastic constants; the second shows how errors on the identification of the zero-depth point can be corrected.

2.1 Strain gauge setup and material elastic constants

First, a reference system is defined as in Fig. 3. The x is aligned with the specimen longitudinal axis, the z points outwards from the upper face of the specimen, and the y follows consequently. A FEM model of the specimen was built in ANSYS [14] (see Fig. 4) and was correlated with the physical system. To do this, an LVDT transducer (resolution: ± 0.001 mm, uncertainty: ± 0.005 mm) was used to measure the vertical deflection at nine points on the tapered region between $x = 250$ mm and $x = 650$ mm, then values were compared with FEM results.

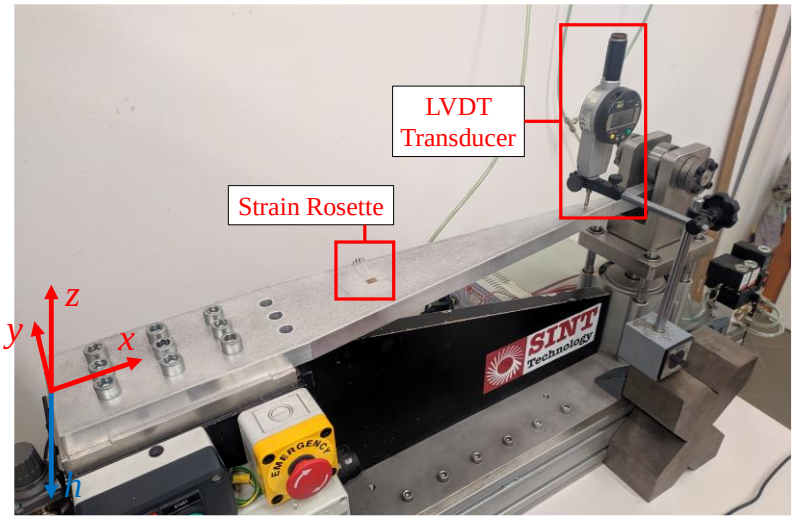

Fig. 3. Specimen reference system and strain rosette calibration procedure. The external load was applied and the specimen deflection in z-direction was measured at nine points on the specimen x-axis with a LVDT transducer. Note that hole steps are drilled towards negative values of z; nevertheless, the hole depth h is defined as a positive quantity.

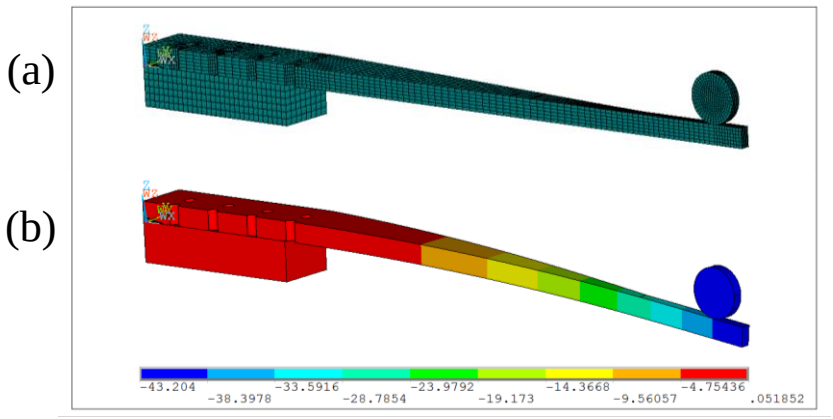

Fig. 4. (a) FEM model of the specimen, built with second-order solid hexahedral elements. An end-displacement is applied to the bearing which transfers the piston load to the specimen. Symmetry about plane xz is exploited to reduce the model computational complexity. Contact elements are used to model the bolted constraints and the interface between the bearing and the specimen end. (b) Deflections in z-direction, as resulting from the FEM model.

According to Euler-Bernoulli beam theory, the tapered region shows a uniform curvature when deflected. This hypothesis was verified by fitting deflection measurements with a quadratic formula: both experimental and FEM deflections were fitted with a maximum residual of less than 0.02 mm, which confirms the assumption. It was also checked that the effects of shear deformation on the curvature of the tapered region were negligible.

As the maximum displacement is imposed, the deflections are independent of the material elastic constants, which can be set freely in the FEM model. Two factors prevent the two deflections from matching: the actual compliance of the bolted end and the actual displacement imposed by the piston, which is not precisely known due to free-plays and compliances. The first can only give rise to a rigid body motion which does not affect the curvature (hence the strains) in the tapered region, so the experimental and modeled curvature must match. Therefore, the end-displacement applied to the FEM model were tuned until the experimental and modeled curvature were the same. Results are shown in Fig. 5.

This process does not require elastic constants nor the applied load to be known, hence it does not depend on errors on those quantities. A sensitivity analysis shows that the experimental curvature is known up to an accuracy of 0.1%, which is likely to be at least as accurate as FEM results. The strain rosette shall measure a positive principal strain that matches the ε_{xx} resulting from the FEM model within tolerance on gage factor values, otherwise the strain gauge setup should be checked. The orientation of the measured principal strains with respect to the specimen longitudinal axis can also be checked. The rosette gage factors may be isotropically scaled to adjust the principal measured strain to its corresponding FEM value. The Poisson ratio ν of the material can be identified from the ratio of the two measured principal strains, up to an accuracy which depends on the variability of gage factors among strain grids.

The applied load is measured with the load cell, and it is equal to 2357 N in this setup; the stress σ_{xx} in correspondence of the strain gauge can be evaluated from beam theory (164.4 MPa). Therefore, the (secant) Young's modulus of the material can be identified as the ratio between σ_{xx} and ε_{xx}. Its accuracy mainly depends on the uncertainties on load cell measurements, whose relative magnitude may be conservatively estimated in the order of a percentage point.

An HBM RY61K strain rosette was glued to the specimen at $x = 292.5$ mm, aligned with the specimen reference system as shown in Fig. 6. Then, this procedure was applied to check the rosette gage factors and the elastic constants of the material. The rosette measured a maximum principal strain of 2362 με, while the FEM analysis showed a $\varepsilon_{xx} = 2347$ με at that point. The difference is less than 1%, hence compatible with the gage factor tolerance specified by the producer; it was compensated by scaling strain measurements. Young's modulus of the material was identified at 70.0 GPa. Results are summarized in Table 1.

Table 1. Results of the correlation between experimental results and the FEM model. The principal strain measured by the strain rosette differs from the FEM strain by less than 1%, which is compatible with the gage factor tolerance. The elastic constants are coherent with a 7075-T651 aluminum and were used in the subsequent HDM procedure.

	Experimental	FEM
Deflections quadratic fit	$-1.176 \cdot 10^{-4}x^2 + +3.55 \cdot 10^{-2}x - 2.69$ [mm]	$-1.176 \cdot 10^{-4}x^2 + +3.75 \cdot 10^{-2}x - 3.02$ [mm]
ε_{xx} at $x = 292.5$ mm	2362 με	2347 με
σ_{xx} at $x = 292.5$ mm	164.4 MPa	
Identified elastic constants	$E = 70.0$ GPa, $\nu = 0.31$	
Strain rosette misalignment	0.25°	

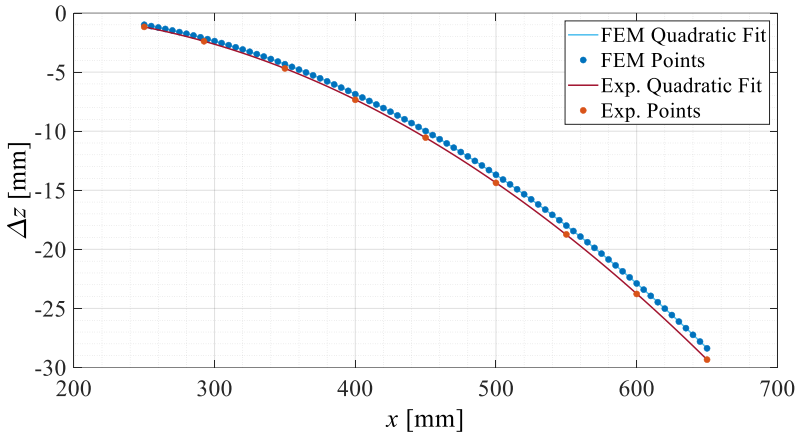

Fig. 5. Specimen deflections in z-direction, along the tapered zone: comparison between experimental measurements (red points) and FEM outputs (blue points) after the calibration procedure which yielded an end-deflection of 38.76 mm. The two datasets were fitted with a quadratic expression, and the FEM applied end-displacement was adjusted until the two expressions yielded the same curvature. A linear difference in the deflections still remains (generated by a different constraint stiffness), but it does not affect strains in the tapered region. The actual constraint stiffness is slightly lower than its FEM prediction.

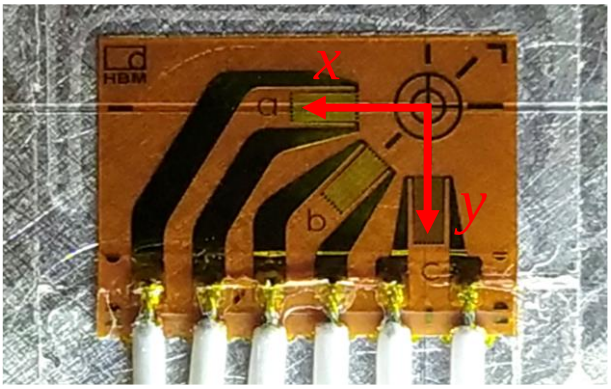

Fig. 6. Strain rosette (HBM RY61K) applied on the upper face of the specimen at $x = 292.5$ mm, aligned with the specimen reference system. Grid naming (**a**, **b** and **c**) is printed on the rosette itself.

2.2 Zero-depth offset errors

An HDM procedure is carried out on the applied strain rosette. Using a $1.6\,\text{mm}$ cutting tool, a maximum depth of $h = 1.2\,\text{mm}$ was reached through 120 increments of $0.01\,\text{mm}$ (a positive depth h is measured oppositely to the z-direction, recall Fig. 3).
The hole step at depth h is performed without the external load applied, so that the relaxed strain measured by the i-th grid $\varepsilon_i^{\mathrm{RS}}(h)$ correspond to the actual residual stress distribution. Then, the deflection is produced through the piston, and the new strains $\varepsilon_i^{\mathrm{F}}(h)$ are recorded. The relaxed strains $\varepsilon_i^{\mathrm{Be}}(h)$ corresponding to the applied bending stresses can be evaluated as follows:

$$\varepsilon_i^{\mathrm{Be}}(h) = \left(\varepsilon_i^{\mathrm{F}}(h) - \varepsilon_i^{\mathrm{F}}(0)\right) - \varepsilon_i^{\mathrm{RS}}(h) \tag{2}$$

Details of the procedure are available in [12]. In this work, only strains $\varepsilon_i^{\mathrm{Be}}(h)$ were considered and are plotted in Fig. 8, as the actual residual stress distribution in the specimen was not analyzed.
The zero-depth point was identified through electric contact between the drilling tool and the metallic specimen surface. By choosing a stress resolution of $0.02\,\text{mm}$, stresses corresponding to $\varepsilon_i^{\mathrm{Be}}(h)$ were evaluated through the IFM (assuming piecewise linear stress distributions) and processed with Tikhonov regularization and Morozov discrepancy principle, according to ASTM E837; they can be found in Fig. 9a. Note that ASTM E837 actually prescribes a maximum hole depth of $1\,\text{mm}$ for the given strain rosette. The largest errors were found precisely in the zone past $1\,\text{mm}$ depth, where the sensitivity of the HDM starts failing, and near the zero-depth point, where other effects arise. For example, in Fig. 7 the effects of imperfect drill surfaces and of tool misalignment are shown: overall, they generate "delayed" strains (as qualitatively shown in Fig. 8b) because a true cylindrical hole starts one or more steps after the first one. Although a precise modeling of a non-cylindrical hole falls outside the axisymmetric hole model used in the HDM, the effect of a $0.02\,\text{mm}$ depth shift (compatible with Fig. 7) of the strains is reported in Fig. 9b: the largest effect is precisely near the zero-depth point.
Knowing this, the actual shift value may be manually tuned in order to reproduce the imposed bending stresses, as shown in Fig. 10a. However, this requires multiple time-consuming evaluations of matrix $\boldsymbol{A}$ in Eq. (1), as it depends on the actual hole depths. Alternatively, another strategy is proposed here. At a first approximation, a small shift in depth Δh is equivalent to a strain variation of $\frac{d\varepsilon}{dh}\Delta h$ at the *same* hole depths. Hence, while keeping matrix $\boldsymbol{A}$ constant and modifying the strains only, Δh can be automatically chosen as the one which minimizes the norm of the stress second-order numerical derivative (to enforce smoothness). Results of this strategy are reported in Fig. 10b. It shall be observed that this procedure yields a significant improvement over uncompensated results, showing absolute errors of less than $10\,\text{MPa}$, even beyond the $1\,\text{mm}$ depth limit prescribed by ASTM E837.

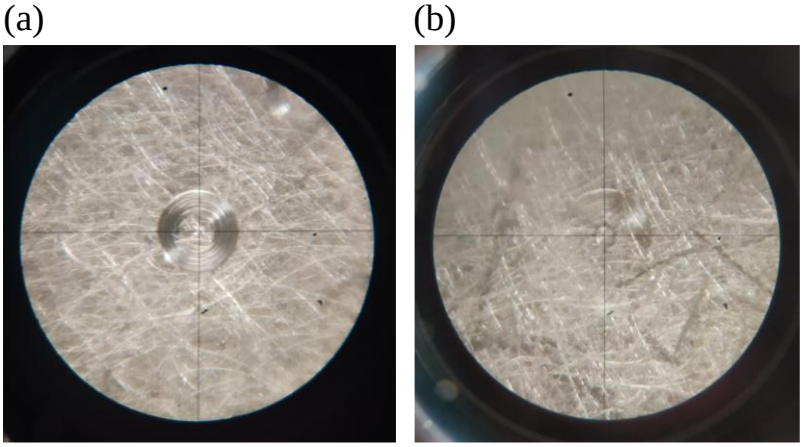

Fig. 7. Examples of situations that generate errors in the reconstruction of residual stresses near the zero-depth point. Images were taken after a 10 μm drilling step from the identified zero-depth point (through electrical contact). (a) Non-planarity of the drilling tool yields a non-flat hole bottom surface. (b) Non-perpendicularity of the drilling axis with respect to the specimen surface yields a non-axisymmetric hole.

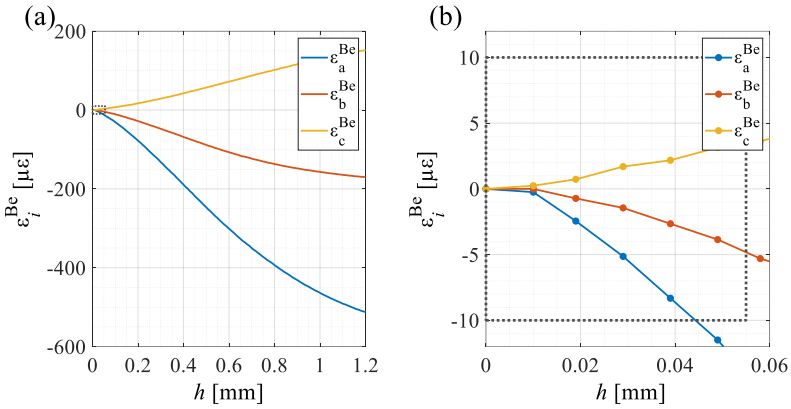

Fig. 8. (a) Bending relaxed strains measured by the three gauges (**a**, **b** and **c**) on the rosette. A dashed grey rectangle highlights a region near the zero-depth point. (b) Zoom on the zero-depth point. A significant jump in the first derivatives of the three curves near the first acquired point ($h = 0.01\ mm$) is qualitatively evident.

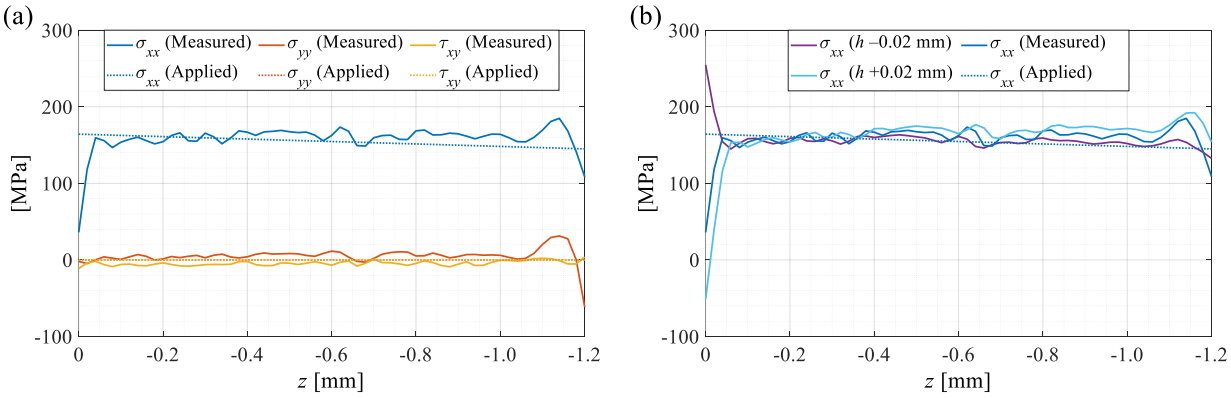

Fig. 9. (a) Bending stress distributions corresponding to measured strains through the hole drilling method inverse problem. Calculation points are evenly spaced with a $0.02\ mm$ step; strain inputs were processed through Tikhonov second-order regularization and Morozov discrepancy principle. (b) Effect of a translation in h of measured strains on the identified σ_{xx}. The most affected zone is near the zero-depth point, while the effect is less pronounced at higher depths.

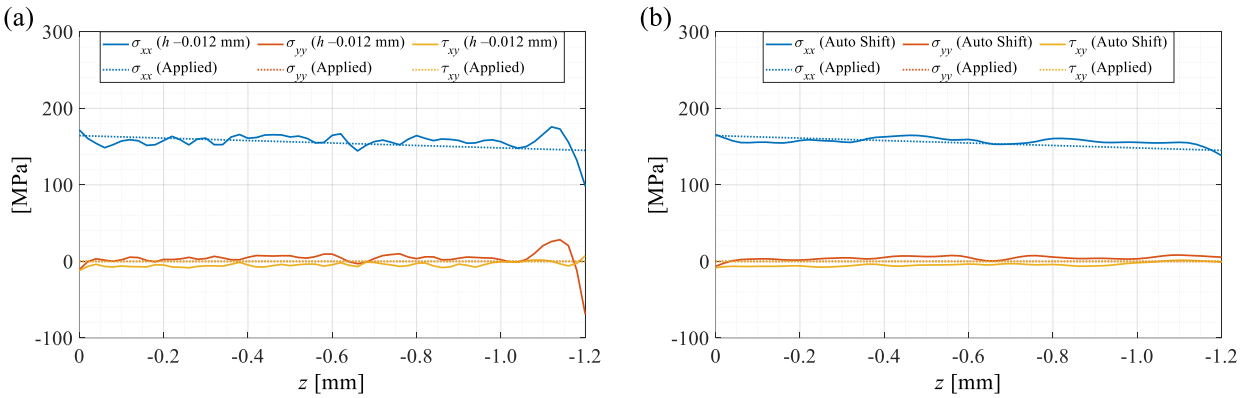

Fig. 10. (a) Bending stress distributions corresponding to measured strains shifted by $-0.012\ mm$, towards the zero-depth point. This specific shifting value has been chosen by manual tuning. (b) Bending stress distributions corresponding to measured strains whose depth shift has been automatically set to $-0.0129\ mm$ by the proposed procedure.

3. Conclusions

A calibration bench for the hole drilling method has been presented, together with some strategies aimed at validating the experimental setup and compensating potential biases in measurements.
In particular:

- It allows a verification of the strain gauge readings which is independent from the uncertainties on the elastic constants of the material and on load measurements.
- It provides feedback on the correct application of the HDM procedure and a quantitative estimation of the errors on the identified residual stresses, as the calculated bending stress distribution can be compared with the applied one.
- It allows the validation of error compensation strategies. For example, it is shown that a zero-depth offset – which affects the identified stress distribution near the specimen surface – can be corrected after that the procedure has been carried out.
- Since the bench permits a *simultaneous* identification of residual and bending stresses, the compensations applied for the bending case (to improve correlation with imposed stresses) can be easily extended to residual stresses, increasing their accuracy.

References

[1] E. M. Beaney, "Accurate measurement of residual stress on any steel using the centre hole method," *Strain*, vol. 12, no. 3, pp. 99–106, 1976, doi: https://doi.org/10.1111/j.1475-1305.1976.tb00194.x.
[2] G. S. Schajer, "Application of Finite Element Calculations to Residual Stress Measurements," *J. Eng. Mater. Technol.*, vol. 103, no. 2, pp. 157–163, Apr. 1981, doi: 10.1115/1.3224988.
[3] G. S. Schajer, "Measurement of Non-Uniform Residual Stresses Using the Hole-Drilling Method. Part I—Stress Calculation Procedures," *J. Eng. Mater. Technol.*, vol. 110, no. 4, pp. 338–343, Oct. 1988, doi: 10.1115/1.3226059.
[4] G. S. Schajer, "Measurement of Non-Uniform Residual Stresses Using the Hole-Drilling Method. Part II—Practical Application of the Integral Method," *J. Eng. Mater. Technol.*, vol. 110, no. 4, pp. 344–349, Oct. 1988, doi: 10.1115/1.3226060.
[5] American Society for Testing and Materials, "Test Method for Determining Residual Stresses by the Hole-Drilling Strain-Gage Method," *West Conshohocken PA*, 2020, doi: 10.1520/E0837-20.
[6] G. S. Schajer, *Practical residual stress measurement methods*. John Wiley & Sons, 2013.
[7] M. Beghini, L. Bertini, and L. F. Mori, "Evaluating Non-Uniform Residual Stress by the Hole-Drilling Method with Concentric and Eccentric Holes. Part I. Definition and Validation of the Influence Functions: Eccentric Influence Functions - Part I," *Strain*, vol. 46, no. 4, pp. 324–336, Mar. 2010, doi: 10.1111/j.1475-1305.2009.00683.x.
[8] M. Beghini, L. Bertini, and L. F. Mori, "Evaluating Non-Uniform Residual Stress by the Hole-Drilling Method With Concentric and Eccentric Holes. Part II: Application of the Influence Functions to the Inverse Problem: Eccentric Influence Functions - Part II," *Strain*, vol. 46, no. 4, pp. 337–346, Mar. 2010, doi: 10.1111/j.1475-1305.2009.00684.x.
[9] G. S. Schajer, "Hole-Drilling Residual Stress Profiling With Automated Smoothing," *J. Eng. Mater. Technol.*, vol. 129, no. 3, pp. 440–445, Jul. 2007, doi: 10.1115/1.2744416.
[10] G. S. Schajer and E. Altus, "Stress Calculation Error Analysis for Incremental Hole-Drilling Residual Stress Measurements," *J. Eng. Mater. Technol.*, vol. 118, no. 1, pp. 120–126, Jan. 1996, doi: 10.1115/1.2805924.
[11] M. D. Olson, A. T. DeWald, and M. R. Hill, "Precision of Hole-Drilling Residual Stress Depth Profile Measurements and an Updated Uncertainty Estimator," *Exp. Mech.*, vol. 61, no. 3, pp. 549–564, Mar. 2021, doi: 10.1007/s11340-020-00679-1.
[12] E. Valentini, M. Beghini, L. Bertini, C. Santus, and M. Benedetti, "Procedure to Perform a Validated Incremental Hole Drilling Measurement: Application to Shot Peening Residual Stresses: Validated IHD Measurement Test Rig," *Strain*, vol. 47, pp. e605–e618, Jun. 2011, doi: 10.1111/j.1475-1305.2009.00664.x.
[13] E. Valentini, M. Benedetti, V. Fontanari, M. Beghini, L. Bertini, and C. Santus, "Fine increment hole-drilling method for residual stress measurement, proposal of a calibrating apparatus," in *Experimental Analysis of Nano and Engineering Materials and Structures*, Springer, 2007, pp. 945–946.
[14] *ANSYS Mechanical Enterprise, Release R2020*. 2020.